Contrib Mineral Petrol (2003) 145: 217–227
DOI 10.1007/s00410-003-0444-3

ORIGINAL PAPER

H.P.Liermann · J. Ganguly

Fe^{2+}–Mg fractionation between orthopyroxene and spinel: experimental calibration in the system FeO–MgO–Al_2O_3–Cr_2O_3–SiO_2, and applications

Received: 27 December 2001 / Accepted: 3 December 2002 / Published online: 11 April 2003

Abstract We have determined the equilibrium Fe^{2+}–Mg fractionation between orthopyroxene and spinel in the ferromagnesium system at 0.9–1.4 GPa, 850–1,250 °C, and also as a function of the Cr/Al ratio of spinel at 1.24 GPa, 1,000 °C. At each P–T condition, the equilibrium value of the distribution coefficient, K_D(Fe–Mg), was constrained by experiments with crystalline starting mixtures, and approaching from both higher and lower initial values. The experimental data have been cast, within a thermodynamic framework, in the form of a geothermometer in the system FeO–MgO–Al_2O_3–Cr_2O_3–SiO_2 (FMACrS). Using the data of O'Neill and Wall (1987) on the thermodynamic properties of Fe^{3+} and Ti^{4+} bearing spinels, we extended the thermometric formulation to account for the effect of these components. However, practical application of the extended formulation is beset with the problem of accurate determination of Fe^{3+} content of natural minerals. Using published data, the thermometric formulation in the FMACrS system has been applied to a number of natural assemblages that have small Fe^{3+} content. The retrieved temperatures are generally higher, on the average by ~60 °C, than those obtained from the olivine-spinel Fe^{2+}–Mg exchange thermometer of O'Neill and Wall, as modified by Ballhaus et al. (1991), but are more compatible with the original temperature estimates by the authors of the publications. The smaller Fe^{2+}–Mg interdiffusion coefficient, D(Fe–Mg), in orthopyroxene compared with those in both olivine and spinel is expected to yield higher temperatures from orthopyroxene–spinel than from olivine–spinel thermometry.

H.P. Liermann
Center for the Study of Matter at Extreme Conditions, Florida International University, Miami 33199, Florida, USA

J. Ganguly (✉)
Department of Geosciences, University of Arizona, Tucson, AZ 85721, USA
E-mail: ganguly@geo.arizona.edu
Tel.: +1-520-621-6006
Fax: +1-520-621-2672

Editorial responsibility: T.L. Grove

Introduction

The Fe^{2+}–Mg fractionation between coexisting orthopyroxene and spinel as a function of temperature (T), pressure (P), and composition (X) is a potentially important geothermometer that is applicable to many terrestrial ultramafic complexes and meteorites, especially the howardite–eucrite–diogenite (HED) suite. Mukherjee and Viswanath (1987) developed a semi-empirical calibration of the dependence of the Fe^{2+}–Mg distribution coefficient, K_D(Fe–Mg), on temperature and Cr^{3+} content of spinel. Their formulation was based on natural and experimental data on the effect of temperature and Cr^{3+} content in spinel on K_D(Fe–Mg). The natural data were taken from a study of Evans and Frost (1975) on a suite of ultramafic rocks that show a widely variable $Cr^{3+}/(Cr^{3+}+Al)$ ratio (henceforth referred to as Y_{Cr}) in spinel, and were believed to have equilibrated at ~700 °C. The experimental data used by Mukherjee and Viswanath (1987) consisted of results from three unreversed experiments at 1,200 °C (Green et al. 1972; Mori 1977; Fujii 1978) on the effect of Cr^{3+} on K_D(Fe–Mg) within the range of $Y_{Cr}=0.10$–0.27. This calibration was subsequently revised by Mukherjee et al. (1990) using additional, but unreversed experimental data on the effect of $Y_{Cr}=0.78$ in spinel on K_D(Fe–Mg) at 1,200 °C, and 1.5 and 2.2 GPa.

Because the calibration of Mukherjee et al. (1990) was based on very limited experimental data, we undertook a systematic experimental study to tightly constrain the K_D(Fe–Mg) between spinel and orthopyroxene in the Cr-free and Cr-bearing systems over a sufficiently large range of temperature and composition. The results of these experiments were utilized to develop a thermometric formulation, within a thermodynamic

framework, and was applied to estimate the Fe–Mg exchange equilibration temperatures between orthopyroxene and spinel in a number of natural samples.

Experimental studies

We synthesized selected starting materials, and carried out Fe^{2+}–Mg exchange experiments between orthopyroxene and spinel at desired P–T conditions using crystalline starting mixtures. All experiments were carried out in a piston-cylinder apparatus using a 3/4'' pressure vessel. Except for two cation exchange experiments, in which talc-glass pressure cells were used, $BaCO_3$ was used as the outer bushing material of the pressure cells. The use of $BaCO_3$ was necessitated by the P–T conditions of the experiments, at which the conventional low-friction salt cells made from either NaCl or CsCl melt. Furthermore, we experienced less thermocouple failures with $BaCO_3$ cells than with talc-glass cells. The frictional behavior of $BaCO_3$ cells was similar to that of CsCl cells (Bose and Ganguly 1995) in that the friction decayed nearly completely after ~48 h, as determined by monitoring the piston intrusion as a function of time (see Bose and Ganguly 1995, for details about piston intrusion measurement and interpretation).

Starting materials

The starting materials for the fractionation experiments consisted of both natural and synthetic spinel and orthopyroxene. The compositions of these phases are summarized in Table 1. The natural orthopyroxene crystals had 51 and 13 mol% of $FeSiO_3$ (Fs). Portions of a single spinel octahedron from Sri-Lanka that contained 2–5 mol% hercynite ($FeAl_2O_4$) were used as starting material of Mg-rich spinel.

Iron-rich orthopyroxene, enstatite, iron-rich spinel and chromite-bearing spinels were synthesized from stoichiometric mixtures of the following oxides (with the indicated level of purity): MgO (99.5%), Fe_2O_3 (99.99%), and SiO_2 (99.9%), Al_2O_3 (99.99%), and Cr_2O_3 (99.8%). In all but one case, which is discussed below, Fe_2O_3 in the oxide mixture reduced to FeO in the reducing environment of graphite capsules. Enstatite was synthesized within boron nitride (BN) capsules. Except for one sample, s-sp09 (Table 1), X-ray powder diffraction scans showed no unintended phase within the products of syntheses experiments. The dimensions of synthetic orthopyroxene and spinel grains were 50–200 and 10–100 μm, respectively. The conditions of the syntheses experiments along with the compositions and cell parameters of the product phases, as determined from electron microprobe analyses and X-ray powder diffraction data, respectively, are summarized in Table 2.

Mössbauer analyses (Table 2) were carried out to determine the Fe^{3+} contents of two synthetic spinels, s-sp09, s-sp14 (Table 2), which were used as starting materials in the fractionation experiments. There was no detectable Fe^{3+} in s-sp14, which has a composition of $Fe_{.49}Mg_{.51}Al_2O_4$, as determined by microprobe analyses and charge balance constraint. However, the iron spinel, s-sp09, which was synthesized in a graphite capsule and had the starting stoichiometry of hercynite, was found to contain 7.8 mol% Fe^{3+} that must have replaced the octahedral Al in the spinel structure. The additional alumina was detected in the powder X-ray diffraction pattern of only the rim of the pellet. Thus, the inner part of the pellet was used for experiments that were intended for the determination of Fe^{2+}–Mg fractionation.

Table 1 Microprobe analyses of natural and synthetic (*s*) orthopyroxenes and spinels (*sp*) used as starting materials in the fractionation experiments; *apfu* atoms per formula unit, on the basis of four cations in orthopyroxene and three cations in spinel

	Opx				Spinel					
	Tel[a]	HO[b]	s-en02	s-px02	sp-r02	s-sp09	s-sp14	s-sp16	s-sp17	s-sp20
wt%										
SiO_2	56.30	51.01	59.50	46.90	0.09	0.06	0.06	0.04	0.01	0.03
TiO_2		0.11								
Cr_2O_3		0.01		0.56	0.38	0.01	0.01	42.14	25.06	59.36
Al_2O_3	0.08	0.89	0.30	0.85	70.10	53.56	63.72	26.96	42.21	12.42
FeO	9.32	30.67	0.11	44.62	0.15	40.66	22.44	18.69	21.02	17.47
Fe_2O_3	0.00	0.00	0.00	0.00	0.00	6.50	0.44	0.00	0.00	0.00
MgO	33.81	16.57	39.97	6.80	28.37	0.01	13.05	11.10	11.19	10.35
MnO	0.05	0.44	0.01	0.05	0.02			0.20		0.42
NiO	0.05	0.00								
CaO	0.32	0.90								
Na_2O		0.01								
Total	99.93	100.61	99.89	99.77	99.09	100.80	99.72	99.12	99.49	100.04
apfu										
Si	1.958	1.965	1.991	1.958	0.002	0.002	0.002	0.001	0.000	0.001
Ti	–	0.003	–	–	–	–	–	–	–	–
Cr	0.000	0.000	0.000	0.018	0.007	0.000	0.000	1.026	0.572	1.531
Al	0.003	0.040	0.012	0.042	1.978	1.856	1.988	0.978	1.438	0.478
Fe^{3+}	0.000	0.000	0.000	0.000	0.000	0.144	0.011	0.000	0.000	0.000
Fe^{2+}	0.271	0.988	0.003	1.558	0.003	1.000	0.485	0.481	0.508	0.477
Mg	1.753	0.951	1.994	0.423	1.012	0.000	0.515	0.509	0.482	0.503
Mn	0.001	0.014		0.002				0.005		0.012
Ni	0.001									
Ca	0.012	0.037								
Na		0.001								
Charge	5.960	5.988	5.997	5.926	3.993	4.000	4.000	4.002	4.005	4.004
$X(Cr)$					0.00	0.00	0.00	0.51	0.28	0.76
$X(Fe^{2+})$	0.13	0.51	0.00	0.79	0.00	1.00	0.49	0.49	0.51	0.49

[a]Opx sample from Telemark, Norway analyzed by Lee and Ganguly (1988)
[b]Opx sample from Central Gneissic Complex (Hollister 1982)

Table 2 Conditions of syntheses experiments and properties of the synthetic phases.Fe^{3+}:CB stand for Fe^{3+} estimated from charge balance

Run no.	Starting composition	Expt. conditions			Expt. product	Cell-parameters X-ray powder diffraction	Composition	
		T (°C)	P (GPa)	Time (h)			Microprobe (Fe^{3+}:CB)	Fe^{3+} (Mössbauer)
s-en02	$MgSiO_3$	1,200	1.5	48	Pure enstatite	a = 18.286 (7) b = 8.838(2) c = 5.193 (2)	$MgSiO_3$	
s-px02	$Fe_{.8}Mg_{.2}SiO_3$	1,200	2.5	48	Intermediate orthopyroxene	a = 18.333 (5) b = 8.998 (2) c = 5.235 (5)	$Fe_{.78}Mg_{.22}SiO_3$	
s-sp09	$FeAl_2O_4$	1,150	2.1	48	Hercynite, corundum	a = 8.1691 (2)	$Fe^{2+}Fe^{3+}_{.16}Al_{1.84}$, $Fe^{3+}/Fe_{total} = 0.14$	80% Inverse, $Fe^{3+}/Fe_{total} = 0.078$
s-sp10	$FeAl_2O_4$	1,150	1.0	48	Hercynite, metallic iron, Al-Fe alloy	a = 8.146 (2)	$FeAl_2O_4$, $Fe^{3+}/Fe_{total} = 0.004$	No Fe^{3+}
s-sp14	$Fe_{.5}Mg_{.5}Al_2O_4$	1,150	1.2	48	Intermediate spinel	a = 8.109 (1)	$Fe_{.49}Mg_{.51}Al_2O_4$, no Fe^{3+}	100% Normal, no Fe^{3+}
s-sp16	$Fe_{.5}Mg_{.5}AlCrO_4$	1,150	1.1	48	Intermediate chromite	a = 8.251 (2)	–	–
s-sp17	$Fe_{.5}Mg_{.5}Al_{1.5}Cr_{.5}O_4$	1,150	1.5	48	Intermediate chromite	a = 8.182 (1)	$Fe_{.49}Mg_{.51}Al_{1.74}Cr_{.26}$	–
s-sp20	$Fe_{.5}Mg_{.5}Al_{.5}Cr_{1.5}O_4$	1,150	1.7	48	Intermediate chromite	a = 8.2977 (7)	–	–

Because of the failure to synthesize it by reduction of Fe_2O_3 in graphite capsule, pure hercynite was synthesized from a stoichiometric oxide mixture in which the required amount of iron was introduced as wüstite. The latter was obtained from the reduction of Fe_2O_3 in an oxygen fugacity controlled furnace at 1 bar, 1,000 °C. The oxide mixture was enclosed in a BN capsule, and subjected to 1.0 GPa, 1,150 °C for 48 h. According to Truckenbrodt et al. (1997), a BN capsule within a pressure cell in the piston-cylinder apparatus maintains the f_{O2} imposed by the starting mixture. The products were found to consist of a mixture of pure hercynite, $FeAl_2O_4$, as determined by Mössbauer analysis (Table 2), along with some (~10–20%) amount of metallic iron, and Fe–Al alloy. This synthetic material, however, was not used in any fractionation experiment, but was used as a microprobe standard (see later).

Fractionation experiments

The design of a typical pressure cell used in the fractionation experiments is illustrated in Fig. 1. Using starting mixtures made of appropriate compositions of orthopyroxene and spinel, the equilibrium distribution at each P–T condition was constrained by approaching it from higher and lower initial values of K_D(Fe–Mg). For experiments below 1,250 °C, reaction kinetics were enhanced by mixing the starting material with a PbO–PbF_2 flux. According to Lee and Ganguly (1987), a flux mixture with 0.55 PbF_2 melted above 750 °C at 2 GPa and dissolved 40–60% of the crystalline material. Thus, the starting material in these experiments were mixed with 5–10 wt% flux with 0.55 PbF_2. No lead was detected in the overgrowth rims in the electron-probe analyses of the experimental products. The conditions and results of the fractionation experiments are summarized in Table 3.

In all fractionation experiments, the pressure was initially raised to 1.7 GPa. After reaching the desired temperatures, the pressure

Fig. 1 Schematic cross section of a typical pressure cell used in Fe^{2+}–Mg fractionation experiments in a piston-cylinder apparatus

Table 3 Summary of experimental data for the fractionation experiments. n_{Fe3+}(Sp)stands for the number of moles of Fe^{3+} in spinel with a total number of three cations. Underlined values represent the most evolved compositions

Run no.	Pressure cell	Expt. conditions			Starting composition[a]			Results					
		T (°C)	P (GPa)	time (h)	Opx + sp (Mass ratio)	X_{Cr}(Sp)	n_{Fe3+}(Sp)	Flux (wt%)	Initial K_D	X_{Fe}(Opx)	X_{Fe}(Sp)	Final K_D	σ (K_D)
KD14 1	$BaCO_3$	1,250	1.40	48	Tele + s-sp09 (40/60)	x	0.02	x	∞	0.48	0.65	1.535	0.039
KD14 2					Tele + s-sp09 (70/30)	x	0.02	x	∞	0.20	0.28	1.575	0.041
KD14 3					HO + sp-r02 (70/30)	x	0.00	x	0.05	0.20	0.27	1.501	0.038
KD14 4					HO + sp-r02 (40/60)	x	0.01	x	0.05	0.16	0.21	1.459	0.038
KD14 5					Tele + sp-r02 (40/60)	x	0.00	x	0.19	0.05	0.08	1.468	0.040
KD07 1	Talk-glass	1,150	1.27	48	Tele + s-sp09 (40/60)	x	0.04	9.5	∞	0.39	0.56	1.972	0.049
KD07 2					Tele + s-sp09 (70/30)	x	0.03	9.5	∞	0.25	0.38	1.774	0.045
KD07 3					HO + sp-r01(70/30)	x	0.01	9.5	0.36	0.21	0.30	1.609	0.041
KD07 4					HO + sp-r01(40/60)	x	0.02	9.5	0.36	0.33	0.45	1.663	0.042
KD15 1	$BaCO_3$	1,050	0.91	120	Tele + s-sp09 (40/60)	x	0.01	7.5	∞	0.48	0.65	2.025	0.050
KD15 2					Tele + s-sp09 (70/30)	x	0.01	7.0	∞	0.32	0.46	1.809	0.045
KD15 3					HO + sp-r02 (70/30)	x	0.00	7.5	0.05	0.34	0.49	1.807	0.045
KD15 4					HO + sp-r02 (40/60)	x	0.00	7.0	0.05	0.23	0.33	1.648	0.042
KD15 5					Tele + sp-r02 (40/60)	x	0.00	7.0	0.19	0.12	0.06	0.503	0.014
KD08 1	Talk-glass	1,000	0.90	168	Tele + s-sp09 (40/60)	x	0.03	10.0	∞	0.50	0.67	2.009	0.050
KD08 2					Tele + s-sp09 (70/30)	x	0.02	10.0	∞	0.37	0.54	1.954	0.049
KD08 3					HO + sp-r01 (70/30)	x	0.02	11.0	0.36	0.40	0.55	1.845	0.046
KD08 4					HO + sp-r01 (40/60)	x	0.00	11.0	0.36	0.30	0.36	1.257	0.031
KD20 2	$BaCO_3$	1,000	1.07	217	Tele + s-sp13 (50/50)	x	0.00	7.5	5.67	0.20	0.35	2.129	0.044
KD20 3		Failed after 17.5			Tele + s-sp13 (70/30)	x	0.00	5.0	5.67	0.17	0.33	2.318	0.059
KD20 4					s-px02 + s-sp13 (50/50)	x	0.02	8.0	0.25	0.56	0.69	1.805	0.045
KD20 5					s-px02 + s-sp13 (70/30)	x	0.03	5.5	0.25	0.57	0.72	1.889	0.048
KD25 1	$BaCO_3$	1,000	0.9	280	s-px02 + s-sp09 (75/25)	x	0.03	6.50	∞	0.74	0.88	2.483	0.065
KD25 2					HO + s-sp09 (70/30)	x	0.06	4.00	∞	0.50	0.78	3.507	0.090
KD25 4					Tele + sp-r02 (50/50)	x	0.02	5.00	0.30	0.00	0.02	12.520	0.352
KD25 5					s-px02 + s-sp14 (80/20)	x	0.01	5.50	0.25	0.62	0.75	1.843	0.047
KD19 1	$BaCO_3$	950	1.01	219	HO + s-sp09 (60/40)	x	0.04	5.5	∞	0.50	0.65	1.907	0.048
KD19 2		Failed after 12 h			Tell + s-sp13 (35/65)	x	0.02	3.7	6.14	0.27	0.47	2.419	0.061
KD19 3					Tell + s-sp13 (55/45)	x	0.01	4.0	6.14	0.24	0.45	2.594	0.065
KD19 4					s-px02 + s-sp13 (55/45)	x	0.02	4.5	0.25	0.50	0.67	2.035	0.051
KD19 5					s-sp02 + s-sp13 (35/65)	x	0.01	5.0	0.25	0.51	0.57	1.296	0.006
KD24 1	$BaCO_3$	850	1.00	839	s-en02 + s-sp09 (50/50)	x	0.01	4.5	∞	0.35	0.51	2.009	0.004
KD24 2					Tele + s-sp13 (50/50)	x	0.00	5.0	5.67	0.25	0.42	2.147	0.003
KD24 3					HO + sp-r02 (40/60)	x	0.00	5.5	0.05	0.15	0.23	1.690	0.002
KD24 4					HO + s-sp13 (50/50)	x	0.00	5.0	1.00	0.34	0.53	2.187	0.004
KD21 3	$BaCO_3$	1,000	1.27	218	HO + s-sp16 (65/35)	0.52	0.01	0.3	1.00	0.28	0.68	5.617	0.142
KD21 4					HO + s-sp16 (35/65)	0.52	0.01	2.5	1.00	0.31	0.68	4.842	0.122
KD21 5					s-px02 + s-sp16 (50/50)	0.52	0.01	2.5	0.25	0.48	0.83	5.180	0.132
KD22 1	$BaCO_3$	1,000	1.26	313	s-en02 + s-sp17 (65/35)	0.26	0.01	2.5	∞	0.20	0.44	3.245	0.082
KD22 2					s-en02 + s-sp17 (35/65)	0.26	0.00	2.5	∞	0.18	0.41	3.197	0.081
KD22 3					s-px02 + s-sp17 (20/80)	0.26	0.00	1.5	0.25	0.39	0.64	2.798	0.069
KD22 5					s-px02 + s-sp17 (50/50)	0.26	0.01	3.5	0.25	0.51	0.73	2.602	0.065
KD23 1	$BaCO_3$	1,000	1.39	288	s-en02 + s-sp20 (30/70)	0.77	0.00	2.0	∞	0.10	0.45	7.154	0.184
KD23 2					s-en02 + s-sp20 (70/30)	0.77	0.00	3.5	∞	0.11	0.49	7.970	0.205
KD23 3					s-px02 + s-sp20 (20/80)	0.77	0.00	2.0	0.25	0.20	0.66	7.878	0.200
KD23 4					s-px02 + s-sp20 (50/50)	0.77	0.00	3.5	0.25	0.20	0.68	8.467	0.216
KD23 5					HO + s-sp20 (50/50)	0.77	0.00	3.0	1.00	0.21	0.68	7.905	0.201

[a] X_{Fe} values: HO = 0.5, Tele = 0.15, s-en02 = 0, s-px02 = 0.8, sp-r01 = 0.05, sp-r02 = 0.02, s-sp09 = 1, s-sp13 = 0.5, s-sp16 = 0.5, s-sp17 = 0.5, (s-sp20) = 0.5

was reduced to the experimental condition of 0.9–1.4 GPa. These pressures corresponded closely to the maximum limiting pressures at the experimental temperatures for the stability of spinel plus orthopyroxene relative to that of garnet plus olivine (in terms of Mg end members, the stability of Opx + Sp assemblage is defined by $4MgSiO_3 + MgAl_2O_4 = Mg_3Al_2Si_3O_{12} + Mg_2SiO_4$). This initial over-pressuring was needed to compact the pressure cell so that the thermocouple was held in position during an experiment. The usual "piston-in" modes led to frequent thermocouple extrusions during the experiments, which suggested that at the relatively low pressure of the experiments the crushable alumina in the top part of the cell did not compact sufficiently to hold the thermocouples in place. Continuous pressure adjustments were necessary during the first 12 h to compensate for the increase of pressure as a result of thermal expansion of the pressure cell and hydraulic oil. Without these adjustments, the increased pressure would have pushed the P–T conditions of the experiment out of the stability field of Opx + Sp.

Temperature was monitored during an experiment by a W3%Re vs. W25%Re (type D) thermocouple that was encased in 99.99% pure alumina tubing. The thermocouple junction was embedded in ZrO_2 cement to avoid contamination, and the thermocouple emf was corrected with a cold-junction correction integrated circuit with a maximum error of 0.5 °C. The emf fluctuation during an experiment corresponded to no more than ±1.5 °C temperature variation. The computer-controlled system is equipped

with an automatic switch that shifts it from an emf to a power-control mode within a split second if the thermocouple fails. The power is automatically controlled at the average value over the last 20 s before the thermocouple failure. In two experiments (KD19 and KD20, Table 3), the thermocouple broke after 17.5 and 12 h, respectively, but the experiments continued by the automatic shift from the emf to power-control mode. Because the power to temperature relation in the experimental set up has been found to be very stable, we assumed that the temperature in each of these experiments corresponded to the recorded emf of the thermocouple before it failed.

The experimental products consisted of euhedral to subhedral grains of orthopyroxenes (~50–150 μm in the elongated direction) that were surrounded by spinels (~20–70 μm diameter), embedded in a matrix of quenched $PbO–PbF_2$ flux with some dissolved components from the starting materials. A back scattered electron (BSE) image of the products showed significant overgrowths on the starting materials (Fig. 2). The $Fe^{2+}/(Fe^{2+}+Mg)$ ratio in the orthopyroxenes vs. that in coexisting spinels at each P–T condition in Cr^{3+}-free and Cr^{3+}-bearing systems are illustrated in Fig. 3a, b, respectively (these types of figures are often referred to as Roozeboom diagrams). In comparing the values of the Fe^{2+}–Mg distribution coefficient, K_D, between the different panels of Fig. 3, it should be noted that pressure and temperature have opposing effects on K_D. The equilibrium fractionation at a P–T condition was constrained on the basis of the most evolved compositions from two opposite sides. These compositions are summarized in Table 3. In a small number of cases, the analyzed compositions from the two sides overlapped considerably. These analyses were rejected for the reasons discussed below. The compositional spread of the symbols in Fig. 3a, b is greater than or equal to the analytical uncertainties.

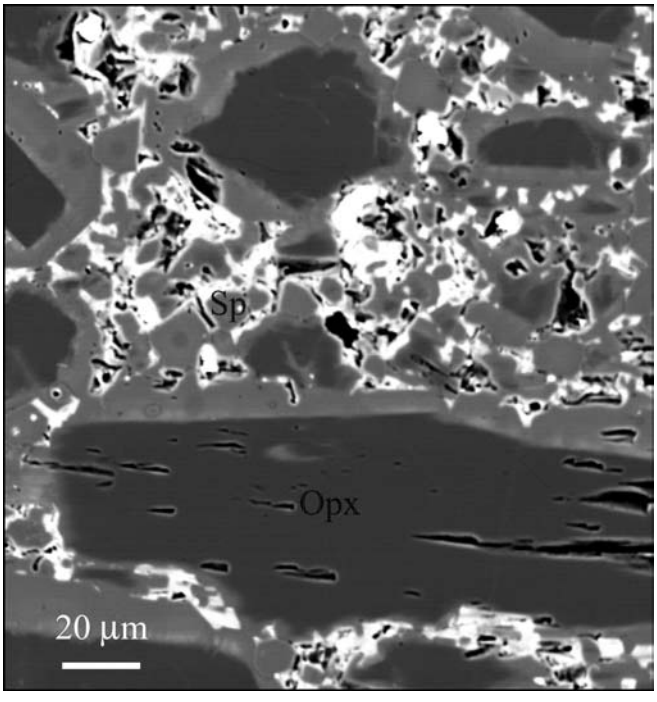

Fig. 2 Back scattered electron image of a portion of a product from a fractionation experiment at 1.27 GPa and 1,150 °C. The image shows a large orthopyroxene crystal (*dark gray*) surrounded by many small spinel crystals (*light gray*). The orthopyroxene shows a light gray rim that is interpreted to be an overgrowth over the core of the seed crystal. The *white material* in the interstitial spaces represents $PbO–PbF_2$ flux

It may be argued (Pattison 1994) that even though the experiments were designed to approach the equilibrium fractionation from two opposing sides, the system did not evolve as desired because of the solution and re-precipitation phenomenon. There are three observations that seem to go against this argument:

1. The compositions that had evolved from the two types of starting mixtures were essentially spread over two different sides in the Roozeboom diagram containing the respective starting compositions (Fig. 3a, b); only a small number of compositions showed overlap.
2. The products of an experiment at 0.79 GPa, 900 °C, which was of insufficient duration, showed considerable separation between the compositions that evolved from the two sides (Fig. 4). This indicates insufficient but uni-directional change of composition towards an equilibrium value. Gessmann et al. (1997) also found progressive change of composition towards equilibrium values in "two-step" experiments on Fe–Mg exchange between garnet and biotite in which the exchange was primarily mediated through solution and re-precipitation. In the "two-step" experiments, the products from the first step were analyzed and recycled at the same P–T condition for additional time.
3. Compositional overlap was also found in a flux-free experiment at 1.4 GPa, 1,250 °C (no. KD14, Table 3).

We, thus, believe that the overlap of compositions in the fractionation experiments were primarily analytical artifacts rather than the results of "path looping" (i.e., precipitation of a phase with a composition that is not in the same side as the starting composition with respect to the equilibrium state). A possible explanation for the problem of compositional overlap is the mixing effect that takes place when the interface between two minerals is tilted with respect to the surface of the probe mount, and the electron beam excites the underlying phase.

Microprobe analyses

The products of syntheses and the fractionation experiments were mounted in epoxy, polished, and analyzed for Mg, Fe, Al, Cr, and Si with wavelength dispersive spectrometers (WDS) in a CAMECA SX50 electron microprobe using 15-kV accelerating voltage and 20-nA beam current. Concentrations of Ti, Mn, and Ca in the minerals were below the detection limit of the electron microprobe. The following standards were used: synthetic hercynite ($FeAl_2O_4$, s-sp10, Table 2) for Fe and Al, synthetic enstatite ($MgSiO_3$, s-en02, Table 2) for Mg and Si, and a natural chromite for Cr. The chromite is from the Tiabaghi Mine, New Caledonia. It was obtained from the United States Natural History Museum (sample no. USNM 117075), and is characterized in the Geostandards Newsletter (1980). The calibration for Fe and Si were tested against a secondary standard of synthetic ferrosilite.

BSE images of run products from experiments with $PbO–PbF_2$ flux showed overgrowth on grains (Fig. 2) that were in most cases smaller than 10 μm. To avoid convolution effects, the electron beam was positioned 3–5 μm away from the grain boundary, in accordance with the analysis of the convolution problem by Ganguly et al. (1988). Only those microprobe data in which the total of oxide wt% were 98.5–101.5 wt% were initially accepted for constraining the equilibrium fractionation. From these, spinel analyses containing more than 0.5 mol% of silicon and orthopyroxene analyses, with a charge deficiency of more than 1%, were rejected as being disturbed by the convolution effect.

Determination of Fe^{3+} content of spinels

The $Fe^{3+}/\Sigma Fe$ in minerals is often determined from the microprobe data by imposing the condition of electroneutrality. However, this procedure also absorbs the error of the analytical data into the

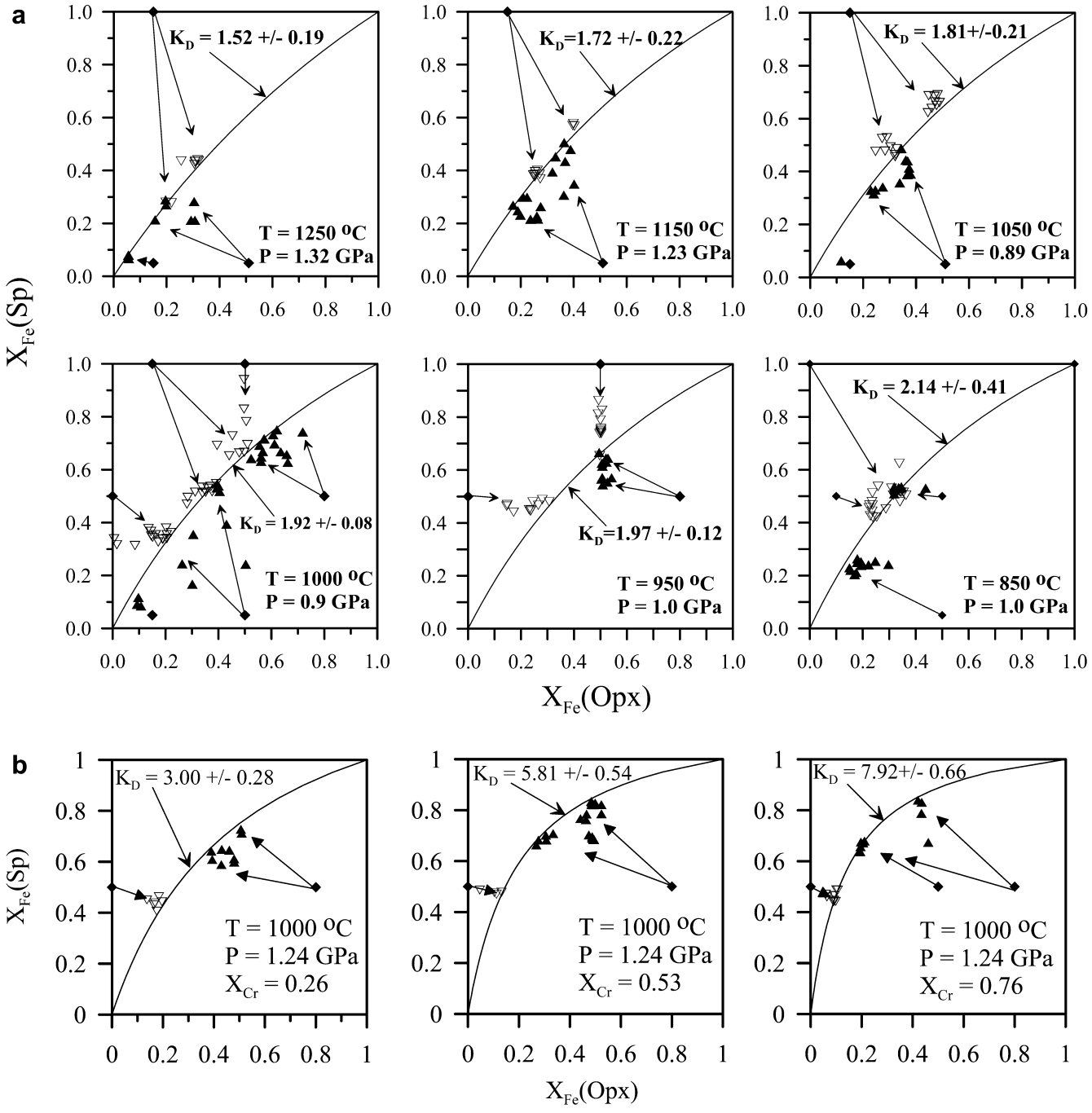

Fig. 3 Roozeboom diagrams showing the compositions of coexisting orthopyroxene and spinel in **a** the Cr^{3+}-free system at different P–T conditions and **b** Cr^{3+}-bearing system at 1.24 GPa, 1,000 °C. K_D represents the inferred equilibrium Fe^{2+}–Mg distribution coefficient. *Filled diamonds* indicate starting compositions, whereas the *open and closed triangles* indicate evolved compositions from the indicated starting compositions. The analytical errors lie within the size of the *symbols*

estimated Fe^{3+} content. Sobolev et al. (1999) found that the charge-balancing procedure tends to overestimate the Fe^{3+} content of a sample. Wood and Virgo (1989), on the other hand, showed that charge-balancing procedure yields a statistically satisfactory estimate of Fe^{3+} content if these are corrected on the basis of results on a set of secondary spinel standards of known Fe^{3+} content. In their work, $Fe^{3+}/\sum Fe$ of the spinel secondary standards was characterized by Mössbauer analyses. In our work, we used the synthetic spinel, s-sp10, for which there is no detectable Fe^{3+} content in the Mössbauer analysis (Table 2), as the primary standard for iron. Comparison between the Fe^{3+} contents determined by Mössbauer spectroscopy and charge balance (CB) constraints of two selected samples (s-sp09 and s-sp14, Table 2) suggests that the latter procedure overestimates the Fe^{3+} content determined on the basis of our microprobe data. The relationship between the Fe^{3+} contents determined according to the two procedures can be expressed as

$$\left(Fe^{3+}/\sum Fe\right)(\text{Moessbauer}) = \left(Fe^{3+}/\sum Fe\right)(\text{CB})/1.60(\pm 0.02) \quad (1)$$

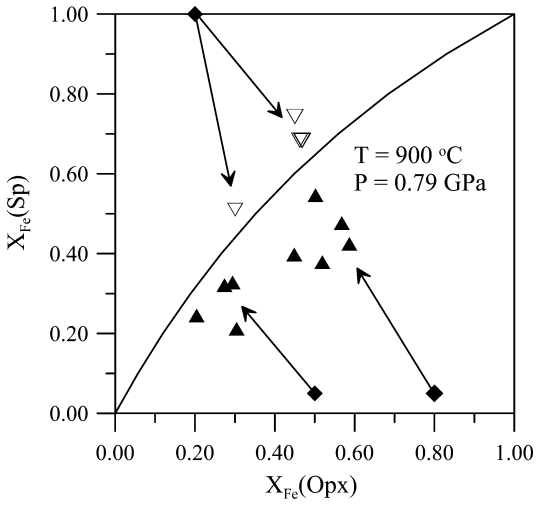

Fig. 4 Roozeboom diagram showing the compositional evolution of coexisting orthopyroxene and spinel in an experiment at 0.79 GPa, 900 °C in the Cr-free system using PbO–PbF_2 flux. The experiment was terminated before the mineral compositions evolved sufficiently towards the equilibrium values. No overlap was found between the evolved compositions from the two sides, which suggests that the compositions from each starting compositions evolved in the directions indicated by the *arrows* without "path looping"

In addition to calculating Fe^{3+} from simple charge balance scheme, we have also used this relation to estimate the Fe^{3+} content in our experimental product.

Thermodynamic analysis

Exchange equilibrium and reciprocal solution

The equilibrium fractionation of Fe^{2+} an Mg between spinel and orthopyroxene may be treated in terms of the exchange equilibrium

$$MgAl_2O_4(Sp) + FeSiO_3(Opx) = FeAl_2O_4(Sp) + MgSiO_3(Opx) \quad (a)$$

We define the distribution coefficient (K_D) of Fe^{2+} and Mg between spinel and orthopyroxene as

$$K_D(Fe-Mg) = \frac{\left(Fe^{2+}/Mg\right)^{Sp}}{\left(Fe^{2+}/Mg\right)^{Opx}}, \quad (2)$$

and a corresponding ratio of activity coefficients of Fe^{2+} and Mg, reflecting their non-ideal interactions within the respective host sites, as

$$K_\gamma(site) = \frac{\left(\gamma_{Fe^{2+}}/\gamma_{Mg}\right)^{Sp}}{\left(\gamma_{Fe^{2+}}/\gamma_{Mg}\right)^{Opx}}. \quad (3)$$

In this work, spinel solid solution involves $Fe^{2+}\leftrightarrow$Mg substitution with or without Al↔Cr substitution. In the Cr-bearing system, spinel is a reciprocal solid solution (e.g., Wood and Nicholls 1978; Ganguly and Saxena 1987) so that the activity coefficient of the components $MgAl_2O_4$ and $FeAl_2O_4$ should incorporate the effect of the homogeneous reciprocal exchange reaction:

$$FeCr_2O_4 + MgAl_2O_4 = MgCr_2O_4 + FeAl_2O_4 \quad (b)$$

In addition, one also needs to account for the effect of disordering between the tetrahedral and octahedral sites of spinel. Ignoring this effect, that is treating Cr-bearing spinel as a two-site reciprocal ionic solution, $^{IV}(Fe^{2+},Mg)^{VI}(Al,Cr)_2O_4$ (with the left superscripts indicating the coordination numbers), and also the effect of very dilute Cr-content in orthopyroxene on K_D, we then obtain (Wood and Nicholls 1978; Ganguly and Saxena 1987)

$$\ln K_D(Fe-Mg) \approx \ln K - \ln K\gamma(site) + \frac{\Delta G^o_{rec}(b)}{RT} Y^{Sp}_{Cr}, \quad (4)$$

where K is the equilibrium constant of the exchange reaction (a), and $\Delta G^o_{rec}(b)$ is the standard state Gibbs energy change of the reciprocal reaction (b). In this derivation, it was further assumed that the Fe^{2+}–Mg interaction within the tetrahedral site of spinel is independent of the Al/Cr ratio in the octahedral site. The data in the Cr-free system (Fig. 3a) suggest that the distribution coefficient is not significantly affected by the change of Fe^{2+}/Mg ratio. This implies that the K_γ(site) term in Eq. (4) is effectively a constant at a given P–T condition. The simplest explanation for this behavior is nearly ideal mixing of Fe^{2+} and Mg in both spinel and orthopyroxene.

Pressure effect on K_D

The polybaric K_D values retrieved from the experimental Fe^{2+}–Mg exchange data were normalized to a uniform pressure of 1.0 GPa according to the following relation.

$$\frac{\partial \ln K_D}{\partial P} \approx \frac{\partial \ln K}{\partial P} = -\frac{\Delta V^o}{RT} \quad (5)$$

The above relation assumes that the end-member (standard state) molar volume change for the reaction (a) is essentially the same as its partial molar volume change. Neither spinel nor orthopyroxene exhibit any volumetric non-ideality of mixing in the Fe^{2+}–Mg binary system, so that the assumption of the equality of the partial and molar volume changes of the reaction (a) is justified in the binary system. In our experiments, the orthopyroxenes were found to contain 2–13 mol% alumina in solid solution. We assume that the substitution of these amounts of Al in orthopyroxene does not significantly affect the difference between the partial molar volumes of the $FeSiO_3$ and $MgSiO_3$ components. This assumption may not be completely justified, but the error introduced by this assumption is likely to be small. Furthermore, because the volumes of the Fe^{2+} and Mg end-member components of a mineral have very similar pressure

dependencies at least up to a few GPa, we assume ΔV^{o} to be independent of pressure. Using the data from Saxena et al. (1993), we estimate $\Delta V^{o} = 121$ J/GPa.

Effect of alumina solubility in orthopyroxene on K_D

Using a simple mixture model for the mixing of Mg, Fe^{2+}, and Al in the octahedral site of orthopyroxene, it can be easily shown (e.g., Ganguly and Saxena 1987) that

$$RT \ln K_D(X_{Al} = 0) = RT \ln K_D + \Delta W_{Al}(X_{Al})^{OPx} \quad (6)$$

where $(X_{Al})^{OPx}$ stands for the mole fraction of Al_2O_3 component in orthopyroxene, and ΔW_{Al} denotes the difference between the $MgSiO_3$–Al_2O_3 and $FeSiO_3$–Al_2O_3 interaction parameters, i.e., $\Delta W_{Al} = W_{Mg-Al} - W_{Fe-Al}$. Berman and Aranovich (1996) have estimated values of these "simple mixture" interaction parameters, which yield $\Delta W_{Al} = 15{,}490$ J/mol at 1.0 GPa.

Treatment of the experimental data

Using Eqs. (5) and (6), and the relevant data on the volumetric (Saxena et al. 1993) and interaction parameters (Berman and Aranovich 1996), we have normalized the $\ln K_D$ values to 1.0 GPa and $X_{Al}(OPx) = 0$ at the different temperatures of our experiments. These $\ln K_D$ values and those without correction for the alumina effect, but normalized to 1.0 GPa, are plotted vs. $1/T$ in Fig. 5 as closed and open symbols, respectively. The triangles stand for the data in which Fe^{3+} was estimated from charge balance, whereas the circles stand for those for which these Fe^{3+} was further readjusted according to Eq. (1). The coefficients for linear regression of each set of data in the four models, according to $\ln K_D = (A + P\Delta V^{o})/RT + B$, are summarized in Table 4. The linear fitting of the data assumes that ΔH^{o} and ΔS^{o} of the exchange reaction (which equal the coefficient of $-(1/RT)$ and BR, respectively) do not change perceptively as a function of temperature, as seems to be case within the range of temperature (850–1,250 °C) encompassed by the experimental data. Given the uncertainty of the experimental data, a more sophisticated treatment of the data incorporating the C_P effects does not seem warranted. It should also be noted that the available C_P values for the iron end members are retrieved from phase equilibrium data in the self-consistent data bases (e.g., Saxena et al. 1993), and not measured calorimetrically, so that the use of these C_P data in isolation of the correlated enthalpy and entropy data from the same data base may introduce errors.

The effect of Cr^{3+} on $K_D(Fe^{2+}$–Mg) is illustrated in the inset of Fig. 5b. Using Eq. (4) and assuming K_γ(site) to be constant, as discussed above, the retrieved values of $\Delta G^{o}_{rec}(b)/R$ are summarized in Table 4 for the two different schemes of Fe^{3+} estimation in spinel, and the corresponding corrections for the effect of alumina solubility in orthopyroxene. These analyses yield a narrow range of values of $\Delta G^{o}_{rec}(b)$ of 19,197, and 21,267 J/mol at 1,000°C (the 1σ uncertainty of any individual regression is ~800 J/mol). There have been several estimates of $\Delta G^{o}_{rec}(b)$ (Evans and Frost 1975; Fabries 1979; Roeder et al. 1979; O'Neill and Wall 1987; Mukherjee et al. 1990; Ballhaus et al. 1991; Kertz 1994). These values range from ~16 to 25 kJ/mol at 1,000 °C.

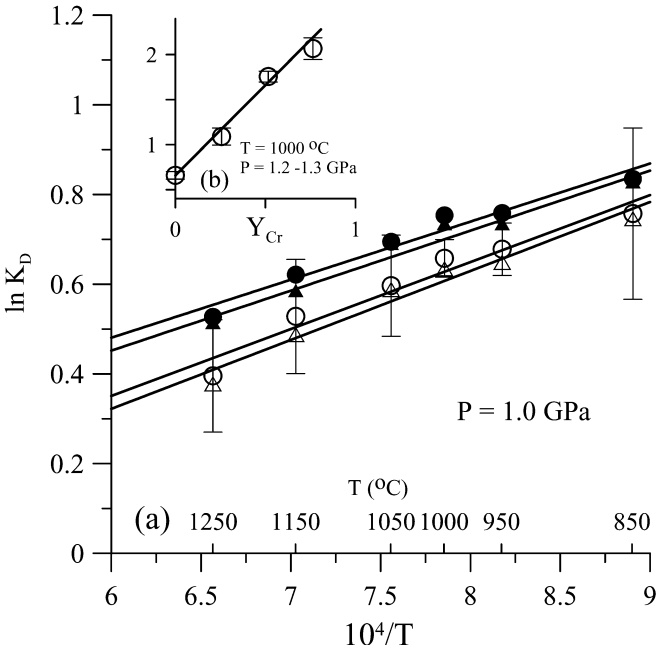

Fig. 5 $\ln K_D$(Fe–Mg) between orthopyroxene and spinel versus **a** reciprocal temperature (K) and **b** Y_{Cr}(Sp), i.e., Cr/(Cr + Al) in spinel at 1.2–1.3 GPa, 1,000 °C. In **a**, the polybaric $\ln K_D$ values have been normalized to a constant pressure of 1.0 GPa. *Vertical bars* represent $\pm 1\sigma$ values. The $\ln K_D$ values with correction for the effect of Al substitution in orthopyroxene are shown as *closed symbols*, whereas those without correction for this effect are shown as *open symbols*. The *triangles and circles* stand for the data in which Fe^{3+} is estimated from charge balance and Eq. (1), respectively

Table 4 Values of the constants in Eq. 8 for the different schemes of treatment of the experimental data. *CB* Charge balance; *Al(OPx)* correction for the effect of alumina solubility in OPx that are correlated with the two schemes of Fe^{3+} estimation in spinel. ± 1standard deviation

Constants	Fe^{3+} correction		Al(OPx)	
	CB	Eq. (1)	Fe^{3+} (CB)	Fe^{3+} [Eq. (1)]
A[a]	–0.6 (±0.1)	–0.55 (±0.13)	–0.351(±0.102)	–0.296 (±0.104)
B[a]	1,450 (±140)	1,372 (±155)	1,217 (±120)	1,174 (±122)
C			1,863	1,863
D	2,484 (±214)	2,558 (±181)	2,345 (±188)	2,309 (±188)

[a]Estimated from the interaction parameters in Berman and Aranovich (1996); no estimate of error is given for these parameters

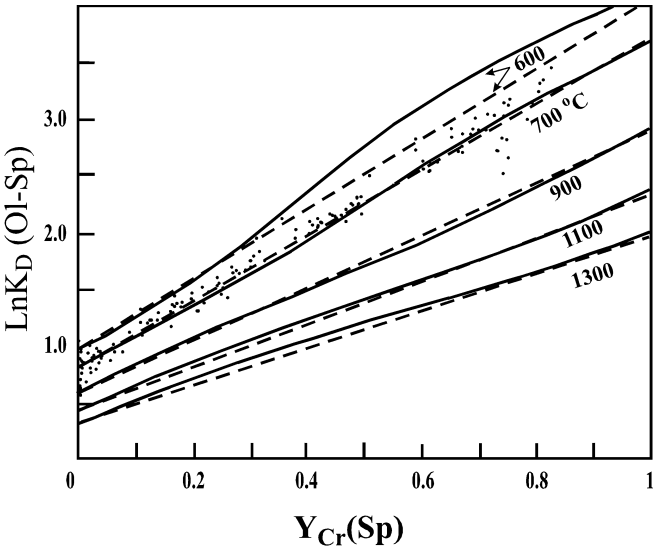

Fig. 6 Comparison of the results on the effect of Cr^{3+} in spinel on $\ln K_D$(Fe–Mg) between olivine and spinel, as derived in this work from the experimental data on the reciprocal reaction (b) in spinel, and a simplified model of its effect on Fe^{2+}–Mg partitioning (*dashed lines*), with those deduced by Sack and Ghiorso (1991; *solid lines*). There is no significant difference between the two formulations at 700–1,300 °C. The *filled symbols* represent the data of Evans and Frost (1975) from a suite of ultramafic rocks, which they inferred to have equilibrated at ~700 °C

Thermometric formulation

The system $FeO–MgO–Al_2O_3–Cr_2O_3–SiO_2$

By comparing the formulations derived from statistical-mechanical and thermodynamic analyses of reciprocal solution, Førland (1964) suggested that the standard state entropy change of a reciprocal reaction should be very small or negligible. We, thus, assume that the value of $\Delta G^{o}_{rec}(b)$, which is derived from the experimental data at 1,000 °C, is independent of temperature within the domain of interest in geological and planetary problems. For the Fe^{2+}–Mg exchange between olivine and spinel, Sack and Ghiorso (1991) formulated a relation between $\ln K_D$(Fe–Mg) and Y_{Cr}(Sp) that incorporated the earlier experimental data of Engi (1983) and Jamieson and Roeder (1984). This relation should be similar to that between $\ln K_D$(Fe–Mg) for the Opx–Sp system and Y_{Cr}(Sp). Figure 6 shows a comparison of our simplified treatment using the reciprocal solution theory and a constant $\Delta G^{o}{}_{rec}(b) = 21{,}267$ J/mol with the more elaborate analyses of Sack and Ghiorso (1991). Also shown for comparison are the natural data on the dependence of $\ln K_D$(Fe–Mg) on Y_{Cr}, as determined by Evans and Frost (1975). These comparative analyses show that our simplified treatment does not introduce any serious error within the temperature–composition space of common geological interest.

Combining Eqs. (4) and (6), and equating $\ln K$ with $\ln K_D[(X_{Al})^{OPx} = (Y_{Cr})^{Sp} = 0]$, which is referred to as $\ln K_D{}^{o}$, we obtain

$$RT \ln K_D \approx RT \ln K_D^{o}(1\text{bar}, T) + P\Delta V^{o} - \Delta W_{Al}(X_{Al})^{OPx} + \Delta G^{o}_{(b)}(Y_{Cr})^{Sp} \quad (7)$$

Thus, expressing $\ln K_D{}^{o}(1\text{ bar},\ T) = A^{o} + B^{o}/T$, $\Delta W_{Al}/R = C$ and $\Delta G^{o}_{(b)}/R = D$, we can write a thermometric equation

$$T(K) \approx \frac{B^{o} + 122P(GPa) - C(X_{Al})^{OPx} + D(Y_{Cr})^{Sp}}{\ln K_D - A^{o}} \quad (8)$$

The values of the A^{o}, B^{o}, C, and D for the different types of treatment of the experimental data are summarized in Table 4. To recapitulate, $(X_{Al})^{OPx}$ and $(Y_{Cr})^{Sp}$ stand for the mole fraction of Al_2O_3 in orthopyroxene [$Al_2O_3/(Al_2O_3 + MgSiO_3 + FeSiO_3)$] and that of Cr in spinel [$Cr/(Cr + Al + Fe^{3+})$], respectively.

Effect of Fe^{3+} and Ti^{4+} content

One may correct for the effect of these additional components using the data from O'Neill and Wall (1987) for the appropriate reciprocal reactions in spinel as long as the coexisting orthopyroxenes have negligible contents of these components. Incorporation of the effects of Fe^{3+} and Ti^{4+} in spinel into the thermometric formulation involves addition of an extra term equal to $\left[\Delta G^{0}_{rec}(c)\ Y_{Fe^{3+}} + \Delta G^{0}_{rec}(d)\ Y_{Ti^{4+}}\right]/R$ to the numerator of Eq. (8), where $\Delta G^{o}rec(c)$ and $\Delta G^{o}rec(d)$ are the standard state Gibbs energy change of the following reciprocal reactions, respectively.

$$MgFe^{2+}_2O_4 + FeAl_2O_4 = MgAl_2O_4 + Fe^{2+}Fe^{3+}_2O_4 \quad (c)$$

$$MgAl_2O_4 + {}^1/_2Fe_2TiO_4 = FeAl_2O_4 + {}^1/_2Mg_2TiO_4 \quad (d)$$

Upon analyzing the available experimental data, O'Neill and Wall (1987) concluded that $\Delta G^{o}_{rec}(c) \approx \Delta G^{o}_{rec}(d) \approx 25{,}250$ J/mol and that these are insensitive to temperature changes. The latter observation is compatible with the general thermodynamic argument made above on the temperature dependence of the standard state Gibbs energy change of a reciprocal solution.

If one accepts the deductions of O'Neill and Wall (1987), and there are no significant amount of Fe^{3+} and Ti^{4+} in orthopyroxene, then the thermometric formulation expressed by Eq. (8) should be modified by adding a term $3037(Y_{Fe^{3+}} + Y_{Ti^{4+}})^{Sp}$ to the numerator to account for the effects of Fe^{3+} and Ti^{4+} in spinel, and calculating $Y_i = i/(Al + Cr + Fe^{3+} + Ti^{4+})$, where $i = Cr$, Fe^{3+}, Ti^{4+}.

Applications to natural assemblages

Although we have proposed a thermodynamic correction for the effect of Fe^{3+} content of spinel on the basis of the work of O'Neill and Wall (1987), practical application of this correction term is beset with the problem of inaccurate determination of Fe^{3+} content in natural samples. Because of the magnitude of the

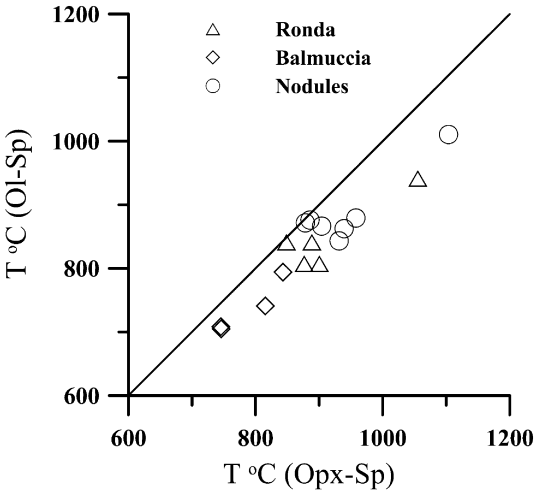

Fig. 7 Comparison of temperatures of samples calculated from the orthopyroxene–spinel thermometer developed in this study, and using the parameters from 4th column of Table 4, with those from the olivine–spinel thermometer of O'Neill and Wall (1987), as modified by Ballhaus et al. (1991)

correction term, an error of 0.01 in the estimated value of $Y_{Fe^{3+}}$ would introduce an error of ~10–20 °C in the estimated value of equilibrium temperature since $\ln K_D$(Fe–Mg) values for natural samples range between ~1 and 2. Using the published compositional data in the literature, we have applied Eq. (8) to a number of terrestrial rocks from alpine peridotites (Shervais 1979; Obata 1980), and ultramafic nodules (Mori 1977; Girod et al. 1981). The Ti^{4+} content of spinels in these samples is negligible, whereas their $Fe^{3+}/(Fe^{3+}+Cr+Al)$ values, as estimated from charge balance, vary between 0.01 and 0.05. A comparison of the temperatures calculated using the values of the A^o, B^o, C, and D parameters from column 4 of Table 4 with those calculated from the olivine-spinel thermometric formulation of O'Neill and Wall (1987), as modified by Ballhaus et al. (1991), is shown in Fig. 7. The chosen set of parameters in Table 4 is based on estimation of Fe^{3+} in spinel from charge balance. Somewhat higher temperatures, on the average by ~20 °C, are obtained by using the set of parameters that correspond to estimate of Fe^{3+} according to Eq. (1) (i.e., column 5 of Table 4). Because the Fe^{3+} of natural samples were estimated by charge balance constraint on the microprobe analyses, the temperatures estimates based on the parameter values in column 4 are probably better than those based on column 5 of Table 4. Without correction for the effect of Al substitution in OPx, the temperature estimates rise further, on the average, by ~25 °C.

As evident from Fig. 7, the temperatures estimated from the OPx–Sp thermometry are usually higher than those estimated from the Ol–Sp thermometry. The original temperature estimates of these rocks by the authors of the papers are also higher than those from Ol–Sp thermometry, usually by similar magnitudes and sometimes even greater. The Fe–Mg interdiffusion data in orthopyroxene (Ganguly and Tazzoli 1994), olivine (Chakraborty 1997) and spinel (Liermann and Ganguly 2002) show that $D(\text{Opx}) < D(\text{Ol}) < D(\text{Sp})$. Thus, the observed discrepancy between the temperatures derived by the OPx–Sp and Ol–Sp thermometers is qualitatively in the right direction because the closure temperature in an exchange pair should be controlled by the mineral with relatively slow diffusion property.

Acknowledgements This research was supported by a NASA grant no. NAG5-10486. We are grateful to Prof. Hans Annersten for the Mössbauer analyses of the spinel samples, and to Prof. Lincoln Hollister for donation of granulite sample from which the orthopyroxene sample, HO, was separated. Drs. Peter Roeder and Martin Engi provided critical, but constructive reviews that led to significant modifications of the paper. J.G. acknowledges the hospitality of the CeSMEC, Florida International University.

References

Ballhaus C, Berry RF, Green DH (1991) High pressure experimental calibration of the olivine–orthopyroxene–spinel oxygen geobarometer: implications for the oxidation state of the upper mantle. Contrib Mineral Petrol 107:27–40

Berman RG, Aranovich LY (1996) Optimized standard state and solution properties of minerals I. Model calibration for olivine, orthopyroxene, cordierite, garnet, and ilmenite in the system FeO–MgO–CaO–Al_2O_3–TiO_2–SiO_2. Contrib Mineral Petrol 126:1–24

Bose K, Ganguly J (1995) Quartz–coesite transition revisited: Reversed experimental determination at 500–1,200 °C and retrieved thermochemical properties. Am Mineral 80:231–238

Chakraborty S (1997) Rates and mechanisms of Fe–Mg interdiffusion in olivine at 980°–1,300 °C. J Geophys Res 102:12317–12331

Engi M (1983) Equilibria involving Al–Cr spinel: Mg–Fe exchange with olivine. Experimental thermodynamic analysis, and consequences for geothermometry. Am J Sci 238-A:29–71

Evans BW, Frost BR (1975) Chrome–spinel in progressive metamorphism—a preliminary analysis. Geochim Cosmochim Acta 39:959–972

Fabries J (1979) Spinel–olivine geothermometer in peridotites from ultramafic complexes. Contrib Mineral Petrol 69:329–336

Førland T (1964) Thermodynamic properties of fused salt systems. In: Sundheim BR (ed) Fused salts. McGraw–Hill, New York, pp 63–164

Fujii T (1978) Fe–Mg partitioning between olivine and spinel. Carnegie Inst Wash Yearbook 76:563–569

Ganguly J, Saxena S (1987) Mixtures and mineral Reactions. Springer, Berlin Heidelberg New York

Ganguly J, Tazzoli V (1994) Fe^{2+}–Mg interdiffusion in orthopyroxene: Retrieval from the data on intracrystalline exchange reaction. Am Mineral 79:930–937

Ganguly J, Bhattacharya RN, Chakraborty S (1988) Convolution effect in the determination of compositional profiles and diffusion coefficients by microprobe step scans. Am Mineral 73:901–909

Gessmann CK, Spiering B, Raith M (1997) Experimental study of the Fe–Mg exchange between garnet and biotite: constraints on the mixing behavior and analysis of the cation-exchange mechanisms. Am Mineral 82:1225–1240

Girod M, Dautria JM, de Giovanni R (1981) A first insight into the constitution of upper mantle under the Hoggar area (southern Algeria): The lherzolite xenoliths in the alkali-basalt. Contrib Mineral Petrrol 77:66–73

Green DH, Ringwood AE, Ware NG, Hibberson WO (1972) Experimental petrology and petrogenesis of Apollo 14 basalt. Proceedings of the 3rd Lunar Science Conference, pp 197–206

Hollister LS (1982) Metamorphic evidence for rapid (2 mm/yr) uplift of a portion of the central-gneiss-complex, coast mountains, BC. Can Mineral 20:319–332

Jamieson HE, Roeder PL (1984) The distribution of Mg and Fe^{2+} between olivine and spinel at 1,300 °C. Am Mineral 69:238–291

Kertz R (1994) Metamorphic crystallization. Wiley, Chichester

Lee HY, Ganguly J (1987) Equilibrium composition of coexisting garnet and orthopyroxene: experimental determination in the system FeO–MgO–Al_2O_3–SiO_2, and applications. J Petrol 29:93–113

Liermann HP, Ganguly J (2001) Compositional properties of coexisting orthopyroxene and spinel in some Antarctic diogenites: implications for thermal history. Meteor Planet Sci 36:155–166

Liermann HP, Ganguly J (2002) Diffusion coefficients of Fe^{2+} and Mg in aluminous spinel: experimental determination and applications to terrestrial and planetary problems. Geochim Cosmochim Acta 66:2903–2913

Mori T (1977) Geothermometry of spinel Lherzolites. Contrib Mineral Petrol 59:261–279

Mukherjee AB, Viswanath MT (1987) Thermometry of diogenites. Mem Natl Inst Polar Res, Spec Issue 46:205–215

Mukherjee AB, Bulatov V, Kotelnikov A (1990) New high P–T experimental results on orthopyroxene–chrome spinel equilibrium and a revised orthopyroxene-spinel cosmothermometer. Proc Lunar Planet Sic Conf XX:299–308

Obata M (1980) The Ronda peridotite: garnet-, spinel-, and plagioclase-lherzolite facies and the P–T trajectories of a high-temperature mantle intrusion. J Petrol 21:533–572

O'Neill HSC, Wall VJ (1987) The olivine–spinel oxygen geobarometer, the nickel precipitation curve, and the oxygen fugacity of the Earth's upper mantle. J Petrol 6:1169–1191

Pattison RM (1994) Are reversed Fe–Mg exchange and solid solution experiments really reversed? Am Mineral 79:938–950

Roeder PL, Campbell IH, Jamieson HE (1979) A re-evaluation of the olivine–spinel geothermometer. Contrib Mineral Petrol 68:325–334

Sack RO, Ghiorso SG (1991) Chromian spinel as petrogenetic indicator: thermodynamics and petrological applications. Am Mineral 76:827–847

Saxena SK, Chatterjee N, Fei Y, Shen G (1993) Thermodynamic data on oxides and silicates. Springer, Berlin, Heidelberg, New York

Shervais J (1979) Thermal emplacement model for the Alpine lherzolite Massif at Balmuccia, Italy. J Petrol 20:795–820

Sobolev VN, McCammon CA, Taylor LA, Snyder GA, Sobolev NV (1999) Precise Mössbauer milliprobe determination of ferric iron in rock forming minerals and limitations of electron microprobe analysis. Am Mineral 84:78–85

Truckenbrodt J, Ziegenbein D, Johannes W (1997) Redox conditions in piston-cylinder apparatus: the different behavior of boron nitride and unfired pyrophyllite assemblies. Am Mineral 82:337–344

Wood BJ, Nicholls J (1978) The thermodynamic properties of reciprocal solid solutions. Contrib Mineral Petrol 66:389–400

Wood BJ, Virgo D (1989) Upper mantle oxidation state: ferric iron contents of lherzolite spinels by ^{57}Fe Mössbauer spectroscopy and resultant oxygen fugacities. Geochim Cosmochim Acta 53:1277–1291